UNCLASSIFIED

AD NUMBER
AD158516
CLASSIFICATION CHANGES

TO:	UNCLASSIFIED
FROM:	CONFIDENTIAL

LIMITATION CHANGES

TO:

Approved for public release; distribution is unlimited.

FROM:

Distribution authorized to U.S. Gov't. agencies and their contractors; Administrative/Operational Use; 27 DEC 1957. Other requests shall be referred to Naval Ordnance Lab., White Oak, MD.

AUTHORITY

NOL ltr 29 Aug 1974 ; NOL ltr 29 Aug 1974

THIS PAGE IS UNCLASSIFIED

AD _____

Reproduced
by the

ARMED SERVICES TECHNICAL INFORMATION AGENCY
ARLINGTON HALL STATION
ARLINGTON 12, VIRGINIA

AD 158516

Armed Services Technical Information Agency

ARLINGTON HALL STATION
ARLINGTON 12 VIRGINIA

FOR
MICRO-CARD
CONTROL ONLY

1 OF 1

NAVORD REPORT

4486

PRESSURE DISTRIBUTIONS ON AN ABMA JUPITER NOSE CONE (13.3 DEGREES SEMI – VERTEX ANGLE) AT NOMINAL MACH NUMBERS 5, 6, 7, AND 8

FC
BAC

27 SEPTEMBER 1957

U. S. NAVAL ORDNANCE LABORATORY
WHITE OAK, MARYLAND

58AA   5196   MAY 1 2 1958

THE

ING

94.

LAW.

NAVORD Report 4486

Aeroballistic Research Report 381

PRESSURE DISTRIBUTIONS ON AN ABMA JUPITER NOSE CONE (13.3 DEGREES SEMI-VERTEX ANGLE) AT NOMINAL MACH NUMBERS 5, 6, 7, AND 8

Prepared by:

E. J. Redman and L. Pasiuk

ABSTRACT: Pressure distributions were obtained on an ABMA JUPITER nose cone (13.3 degrees semi-vertex angle) at nominal Mach numbers of 5, 6, 7, and 8 in the NOL 12 x 12 cm Hypersonic Tunnel No. 4. These distributions were measured along model meridians that were spaced 45 degrees apart, and were taken for yaw angles ranging from 0 to 7.5 degrees. The tabulated data are given and plots are presented to show the chief characteristics of the data. A limited amount of pressure data from tests of a sphere model is included for comparison.

U. S. NAVAL ORDNANCE LABORATORY
WHITE OAK, MARYLAND

1

NAVORD Report 4486   27 September 1957

The hypersonic pressure distributions presented in this
report are among the first to be obtained at NOL on blunt-
body shapes. This investigation of an Army Ballistic
Missile Agency (ABMA) JUPITER nose cone was sponsored
by the U. S. Army and was performed under Task Number
NOL-300. Results presented herein are intended to fa-
cilitate heat-transfer computation.

This document may include technical data and other in-
formation which may be proprietary to parties other than
the Government and, therefore, the transmission by the
Department of the Navy of this document is not to be
regarded, by implication or otherwise, as licensing or
conveying any rights or permission to the recipient or
any other person or corporation gaining access to this
document to use for commercial purposes, as distinguished
from Government purposes, the said technical data or
information disclosed herein.

The authors wish to acknowledge the contributions of
Mr. J. A. Iandolo who was responsible for the design of
the model and Mr. R. H. Garren, Jr., who participated
in the tests and was responsible for the details of the
test preparation.

                          W. W. WILBOURNE
                          Captain, USN
                          Commander

                          R. KENNETH LOBB
                          By direction

CONTENTS

ILLUSTRATIONS

SYMBOLS

M — free-stream Mach number

p — static pressure on model surface

p_a — ambient (free-stream static) pressure

p_b — base pressure

p_o' — Pitot pressure

r — radius of spherical nose (0.385 inches)

Re — free-stream Reynolds number

S — length along model profile, inches; measured from the intersection of the model axis with the spherical nose

S' — length along model profile, inches; measured from the stagnation point on the yawed model

ϵ — yaw angle, degrees; angle between the relative wind vector and the model axis

η — angle between the model axis and a normal to the surface of the spherical nose, degrees; equals S/r radians

η' — S'/r radians

η_b — angle between the model axis and a normal to the surface of the spherical base, degrees

θ — semi-vertex angle of a cone

ϕ — roll angle, degrees; angle between ϕ_0 and the meridian of orifices, Numbers 5-24 (Figure 1)

ϕ_0 — reference meridian defined by the intersection of the windward surface of the model with the plane of yaw

PRESSURE DISTRIBUTIONS ON AN ABMA JUPITER NOSE CONE
(13.3 DEGREES SEMI-VERTEX ANGLE) AT NOMINAL
MACH NUMBERS 5, 6, 7, AND 8

INTRODUCTION

1.   The choice of nose shape for ballistic missiles of
intermediate range is governed largely by considerations
of aerodynamic heating and stability. Blunt bodies are
relatively favorable in regard to heating, but do not
have good stability characteristics. In these respects,
the spherically-blunted cone represents a compromise
configuration. Since theory does not define the pres-
sure gradients on such bodies with sufficient accuracy
for heat-transfer computation, experimental pressure
measurements are needed. Experimental pressure distri-
butions for a series of sphere cones at M - 5.8 are
available in reference (a). The investigation reported
herein presents experimental pressure distributions for
an ABMA JUPITER nose cone taken over a nominal Mach
number range of 5 to 8 in several meridian planes of
the model and over a moderate range of yaw angle.

Construction and Installation of the Model

2.   The pressure model of the JUPITER nose cone had a
base diameter of 2 inches as shown in Figure 1. Pre-
liminary tests with solid models of several sizes in-
dicated that this pressure model should be free from
the effects of shock reflection and of boundary-layer
separation from the wall of the hypersonic tunnel.
The preliminary tests consisted in taking schlieren
photographs over the expected range of test conditions.
A sketch of the pressure model is given in Figure 1,
which shows that the orifices on the spherical nose
were located alternately along two diametrically-
opposite meridians of the model. The model shell was
made of mild steel for ease of manufacture, and was of
integral construction except for the base, which was a
separate spherical segment to which a 0.69-inch O.D.
x 7 3/4-inch hollow sting had been rigidly attached.
The base was threaded into the conical portion of the
model shell to assemble the model. Stainless steel
pressure tubes of 0.025-inch I.D. were finished flush
with the model surface to form orifices normal to the
surface. Internal tubes of 0.042-inch I.D. were con-
tinued to points just beyond the end of the sting.
The use of stainless steel tubing was a precaution

against tube leakage at low test pressures and high operating temperatures.

3.   Figure 2 shows the model mounted in the 12 x 12 cm Hypersonic Tunnel. The model holder consisted basically of a circular rod normal to the sting. A sleeve on the inner end of this rod engaged the sting by means of set screws, as shown in Figure 2, and permitted pre-determined roll increments of ± 45 degrees to be set by matching scribe marks. The rod was locked outside the tunnel door to maintain the yaw angle of the model. As can be seen in Figure 3, a M. C. Clinometer was attached to the rod outside the tunnel to set the yaw angle. Stainless steel tubes of 0.062-inch I.D. were silver-soldered over the leads from the model and were passed without support (approximately 14 inches) down the diffuser section of the tunnel. These tubes exited from the tunnel through a small plenum chamber to provide additional space for flexing the tubes.

4.   For the maximum yaw angle setting, the center of the model nose moved approximately 1 inch off the centerline of the tunnel in the plane perpendicular to the nozzle surface. The axis of rotation in yaw was 6 inches (3 calibers) downstream from the model base.

Test Instrumentation and Operating Conditions

5.   Figure 3 shows the general arrangement of the test instrumentation. In the lower foreground of the photograph are shown two eleven-position rotary "O-ring" vacuum valves of NOL design. The tubing from the first 21 orifices (Figure 1) was connected to these two valves, and the pressures were read to ± 0.1 mm Hg. on two Wallace and Tiernan absolute Hg manometers of one atmosphere range. Tubes from the three orifices on the base sphere-segment were individually connected to oil manometers (reference b) having a common reference vacuum and a range equivalent to 40 mm Hg. These oil manometers (not included in Figure 3) were read to ± 0.002 mm Hg.

6.   The NOL 12 x 12 cm Hypersonic Tunnel No. 4 is a vertical closed-jet tunnel having a Mach number range of 5 to 10 using an adjustable water-cooled wedge nozzle (Figure 2). A nozzle of this type is described in reference (c). For tests of relatively long duration, the large mass-flow requirements near M - 5 make it advisable to set actual Mach numbers consistently higher than the nominal values of 5, 6, 7, and 8. The tunnel conditions applicable to the present tests were:

Mach Number	Supply Pressure (atmospheres)	Supply Temperature (degrees, Rankine)	Free-stream Reynolds Number per Foot
5.4	6.00	645	3.48×10^6
6.3	10.12	888	2.48×10^6
7.2	12.14	1063	1.57×10^6
8.2	25.16	1383	1.53×10^6

7.   The above Mach numbers were obtained as follows: For each setting of the nozzle, the model was retracted toward the wall and Pitot and static probes were mounted at the normal position of the model nose. The Rayleigh formula was applied to the probe pressures to yield the test Mach number. With the model restored to its test position, the reading of the orifice on the model axis duplicated the Pitot-pressure reading obtained from the probe.

RESULTS AND DISCUSSION

8.   Figure 4 shows the location of the bow shock for $M = 6.1$ at zero yaw. This figure is a schlieren photograph of the flow about a 2 1/4-inch base-diameter solid model (with 1/2 inch diameter sting) used in the preliminary tests noted in paragraph 2.

9.   Figure 5 presents the zero-yaw pressure distributions obtained from orifices on the spherical nose and immediately behind its tangency $(S/r = 1.340)$ with the cone. A Newtonian distribution curve (reference d) has been included as a reference for the experimental variation of surface pressure. It may be noted that adjacent points on the plot (10 degree intervals on the sphere) present data from opposite meridians of the model (Figure 1). These pressure distributions show very little variation with Mach number and depart abruptly from the "Newtonian" trend as the point of tangency $(S/r = 1.340)$ is approached.

10.   Figure 6 gives a comparison of the pressure distribution on the spherical nose of JUPITER with the distribution obtained on a 1.75-inch diameter sphere model. The JUPITER nose data tend generally to be somewhat higher than the data shown for the complete sphere. In particular, the presence of a conical afterbody appears to increase substantially the pressures measured on a sphere at stations immediately ahead of the point of tangency.

11.   Figures 7, 8, and 9 show pressure distributions in the yaw plane of the spherical nose at $M = 5.4$, 6.3, and 7.2, respectively. All curves drawn on these three figures are faired experimental curves.

The orifice locations at zero yaw are denoted by darkened
circles. Since S' allows for an effective shift in ori-
fice location with yaw, the data for all yaw angles might
be expected to define a single experimental curve in each
figure. This correlation of all yaw data into a single
curve is reasonably well achieved over approximately the
first 57 degrees (S'/r < 1.000) of the sphere. At larger
angular positions, there is an additional systematic yaw
effect due, presumably, to the presence of the cone.
With ϵ = 7.5 degrees, the point of tangency on the lee-
ward meridian (ϕ = 180 degrees) moves rearward to a
location 84.2 degrees (S'/r = 1.470) from the stagnation
point. For this case, the experimental pressure distri-
bution (as faired by the lower curve in Figures 7, 8, and
9) is significantly below the zero-yaw data and, conse-
quently, has shifted toward the sphere distribution of
Figure 6. The corresponding forward movement of the
point of tangency on the windward meridian (ϕ = 0 degrees)
to a location 69.2 degrees (S'/r = 1.208) from the stag-
nation point is accompanied by a substantial increase in
the experimental pressure distribution (as faired by the
upper curve in Figures 7, 8, and 9) above the zero-yaw
data. It is of interest that these well-defined regions
of cone influence shown in Figures 7, 8, and 9 are prac-
tically identical and, therefore, independent of Mach
number and Reynolds number within the range of test con-
ditions (paragraph 6).

12. Figure 10 presents surface pressures in the yaw-plane
of the cone for M = 5.4, 6.3, and 7.2 at zero yaw and
maximum (ϵ = 7.5 degrees) windward and leeward (ϕ = 0 and
180 degrees) yaw. The symbols for the zero-yaw data have
been shaded for the sake of clarity. Newtonian (refer-
ence d) reference levels of cone pressure are included
at M = 5.4 for the three yaw conditions noted above.
Also included is the level of ambient pressure, p_a, corres-
ponding to M = 5.4. These reference levels are given as a
convenience in orienting the measured pressures, and are
not intended as a basis for comparison with the experimental
values shown. It will be noted that, in terms of S/r,
the plot has been extended around the base corner of the
model to locate the pressures measured on the spherical
base (orifices numbers 22, 23, and 24 of Figure 1). These
pressures remained essentially constant over the yaw angle
range of the tests. The shaded interval of S/r between
the sting juncture and the base center shows the location
and extent of the geometrical blockage of the base region
introduced by the sting.

13. In Figure 10, the cone pressures tend generally to
decrease for increasing Mach number, with the larger

decrease occurring between M = 5.4 and M = 6.3. This variation of pressure with Mach number (or Reynolds number, paragraph 6) is appreciable with respect to the pressure changes on the cone that are associated with differences in surface inclination (ϵ and ϕ). The spread of cone pressure with Mach number for the three yaw conditions develops abruptly aft of the tangency point and remains roughly constant over most of the cone length.

14. Figure 11 gives a comparison of a portion of the present data with results given in reference (a) for a sphere-cone model. The cone-surface inclinations ($\theta + \epsilon$) of 20.8 degrees for JUPITER and 20 degrees for the sphere-cone of reference (a) are comparable, and the use of the ratio, S'/r, correlates the two sets of data in terms of relative distances from the stagnation points on the spherical noses. The data show good agreement.

15. Figures 12 and 13 show transverse pressure distributions around the spherical nose of the JUPITER model at ϵ = 2.5 degrees. Additional distributions at S/r = 1.396 and 7.41 (Figure 13) have been included to represent pressures obtained on the cone. The data variations shown in these figures for the various S/r stations are essentially linear and straight (solid) lines have been faired through the data. Horizontal dash lines give the pressure levels around the model at zero yaw as reference values. For the M = 6.3 and 7.2 data of Figure 13, these faired lines are higher than those drawn for the M = 5.4 and 8.2 data of Figure 12 by approximately 1 percent of the Pitot pressure. Considered both separately and jointly, Figures 12 and 13 indicate the absence of any general Mach number effect on these distributions.

16. Figure 14 presents transverse pressure distributions on the spherical nose at ϵ = 7.5 degrees and M = 5.4, 6.3, and 7.2. To obtain the curves shown in this figure, local surface inclinations (η') at the orifices under combined conditions of yaw and roll were computed from the geometrical relationship

$$\cos \eta' = \cos \epsilon \cos \eta + \sin \epsilon \sin \eta \cos \phi \qquad (1)$$

which has been adapted from Equation (3) of reference (e). With $S'/r = \eta'$ (radians), pressure values were taken from the experimental distribution in the yaw plane (Figure 9) at M = 7.2 to afford comparison with measurements made in other meridian planes. The M = 5.4 data of Figure 7 would have served equally well. On

the whole, the data of Figure 14 show reasonable agreement with these semi-empirical curves. It is thought that the deviations of the data from these curves are due to experimental error, since the curves involve only the assumption that pressures are distributed symmetrically around the stagnation point on a sphere.

17. The tabulated data for these tests are given in Tables I through IV, and the plots discussed above are intended to present the chief characteristics of these data. This tabulation is so arranged that the designation, ϕ - 0 degrees, consistently denotes data obtained with the orifices windward in the plane of yaw, so that orifices numbers 1, 2, 3, and 4 of Figure 1 are, in effect, reflected about the model axis. Therefore, in using the data, all orifices of the spherical nose may be taken to lie along the model meridian defined by orifices numbers 5 through 24 with the same angular positions, η, given in Figure 1. The yaw angles, ϵ, as listed include an allowance for inclination in the nozzle flow. Pertinent test conditions are noted in paragraph 6. The M - 8.2 data have been tabulated in Table IV for ϵ - 0 and 2.5 degrees only.

18. The data as tabulated are referenced to the Pitot pressure for each tunnel run, i.e., for each roll position, ϕ, at a given Mach number. It is believed that the use (at zero yaw) of the number 5 orifice (Figure 1) on the model to monitor the Pitot pressure in the course of each tunnel run was not fully satisfactory and introduced some scatter into the data.

CONCLUDING REMARKS

19. Pressure distributions were obtained on the ABMA JUPITER nose cone at nominal Mach numbers of 5, 6, 7, and 8 and for yaw angles ranging from 0 to 7.5 degrees. These distributions were measured along model meridians that were spaced 45 degrees apart.

20. The pressure distributions on the spherical nose of this configuration do not show any definite effect of Mach number. This statement applies also to that region of the sphere on which pressures are modified by the presence of a conical afterbody. Pressures in this region are influenced systematically by the yaw of the cone, but the forward extent of the region appears to remain fixed at 57 degrees from the stagnation point under all conditions of yaw.

21. On the cone, the decreases in pressure with increasing
Mach number are appreciable as compared with the pressure
changes due to yaw. The pressures vary only slightly with
increasing length along the aftermost portions of the cone
and are well below the pressures existing at the tangency
of the spherical nose with the cone. The Mach number ef-
fect on the cone pressures does not propagate forward of
the tangency point.

REFERENCES

(a) Machell, R. M., O'Bryant, W. T., "An Experimental
Investigation of the Flow Over Blunt-Nosed Cones at
a Mach Number of 5.8," GALCIT Hyp. Res. Proj. Memo
No. 32, June 1956

(b) Kendall, J. M., "Equipment and Techniques for Making
Pressure Measurements in Supersonic Wind Tunnels at
Mach Numbers up to 5.0," NAVORD Report 2580, Aug 1952

(c) Wegener, P. P., Lobb, R. K., Winkler, E. M.,
Sibulkin, M., and Staab, H. C., "NOL Hypersonic
Tunnel No. 4 Results V: Experimental and Theoretical
Investigation of a Cooled Hypersonic Wedge Nozzle,"
NAVORD Report 2701, April 1953

(d) Lees, L., and Kubota, T., "Inviscid Hypersonic Flow
Over Blunt-Nosed Slender Bodies," Jour. Aero. Sci.,
Vol. 24, No. 3, March 1957

(e) Grimminger, G., Williams, E. P., and Young, G. B. W.,
"Lift on Inclined Bodies of Revolution in Hypersonic
Flow," Jour. Aero. Sci., Vol. 17, No. 11, Nov 1950

13.32°

0.385
SPHERICAL-R

1.539
SPHERICAL-R

2.000 DIA

3.309
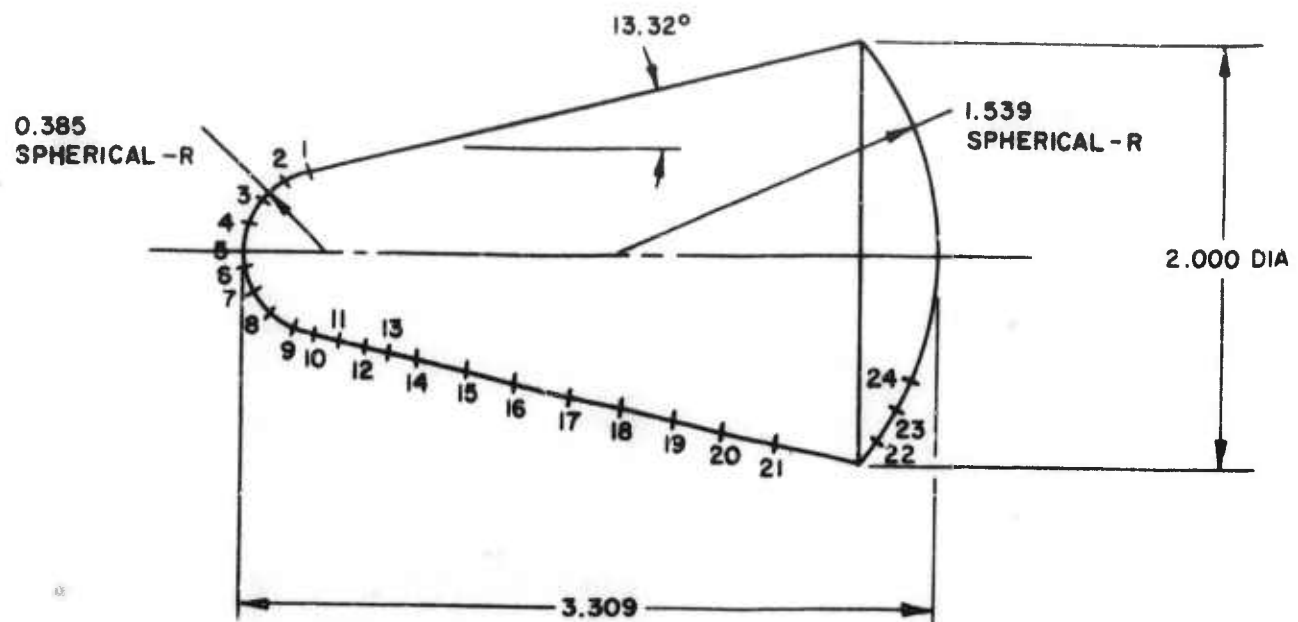
ALL DIMENSIONS IN INCHES UNLESS NOTED OTHERWISE

ORIFICE LOCATIONS

ORIFICE NO.	$\frac{s}{r}$	η NOSE SPHERE	ORIFICE NO.	$\frac{s}{r}$	ηb BASE SPHERE
1	1.396	"80°"	13	2.54	
2	1.047	60°	14	2.87	
3	0.698	40°	15	3.52	
4	0.349	20°	16	4.17	
5	0.000	0°	17	4.82	
6	0.174	10°	18	5.47	
7	0.523	30°	19	6.12	
8	0.872	50°	20	6.76	
9	1.221	70°	21	7.41	
TANGENCY	1.340	76.68°	CORNER	8.39	41°
10	1.571	"90°"	22	8.77	35.5°
11	1.900		23	9.22	29.0°
12	2.220		24	9.64	23.0°

FIG. I SKETCH OF MODEL SHOWING ORIFICE LOCATIONS
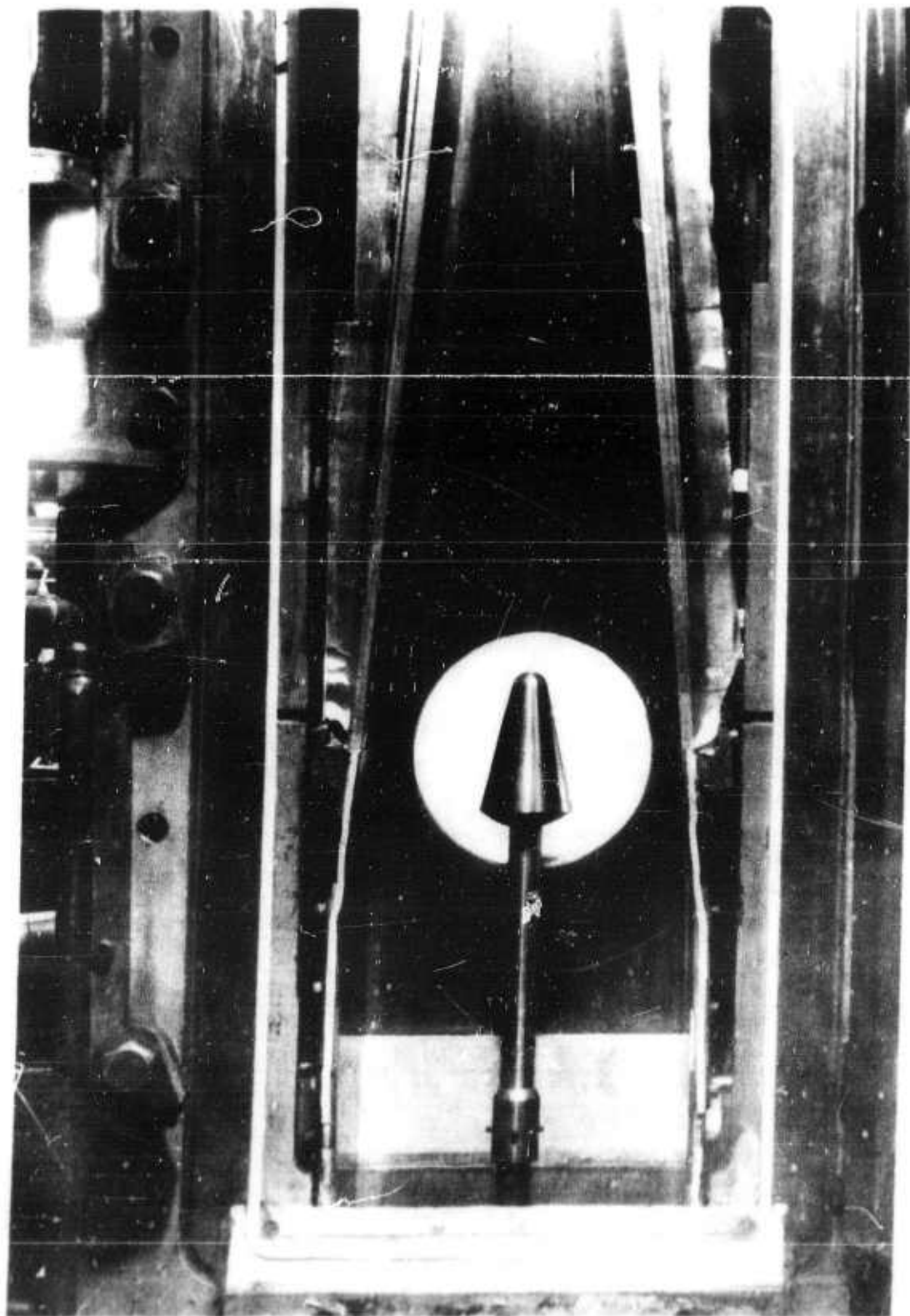
FIG. 2 PHOTOGRAPH OF MODEL MOUNTED
IN TUNNEL
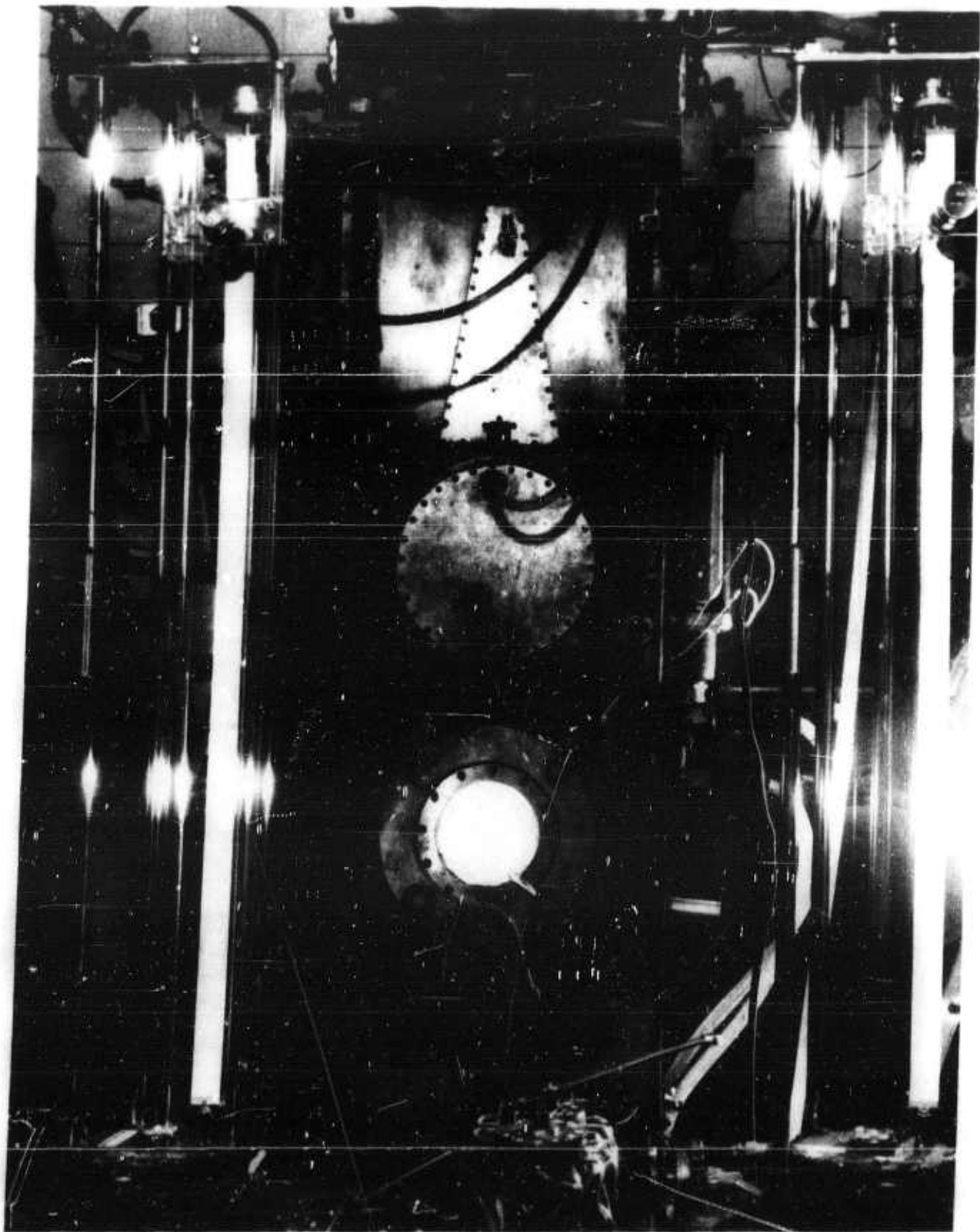
FIG. 3 PHOTOGRAPH OF ARRANGEMENT OF
TEST INSTRUMENTATION
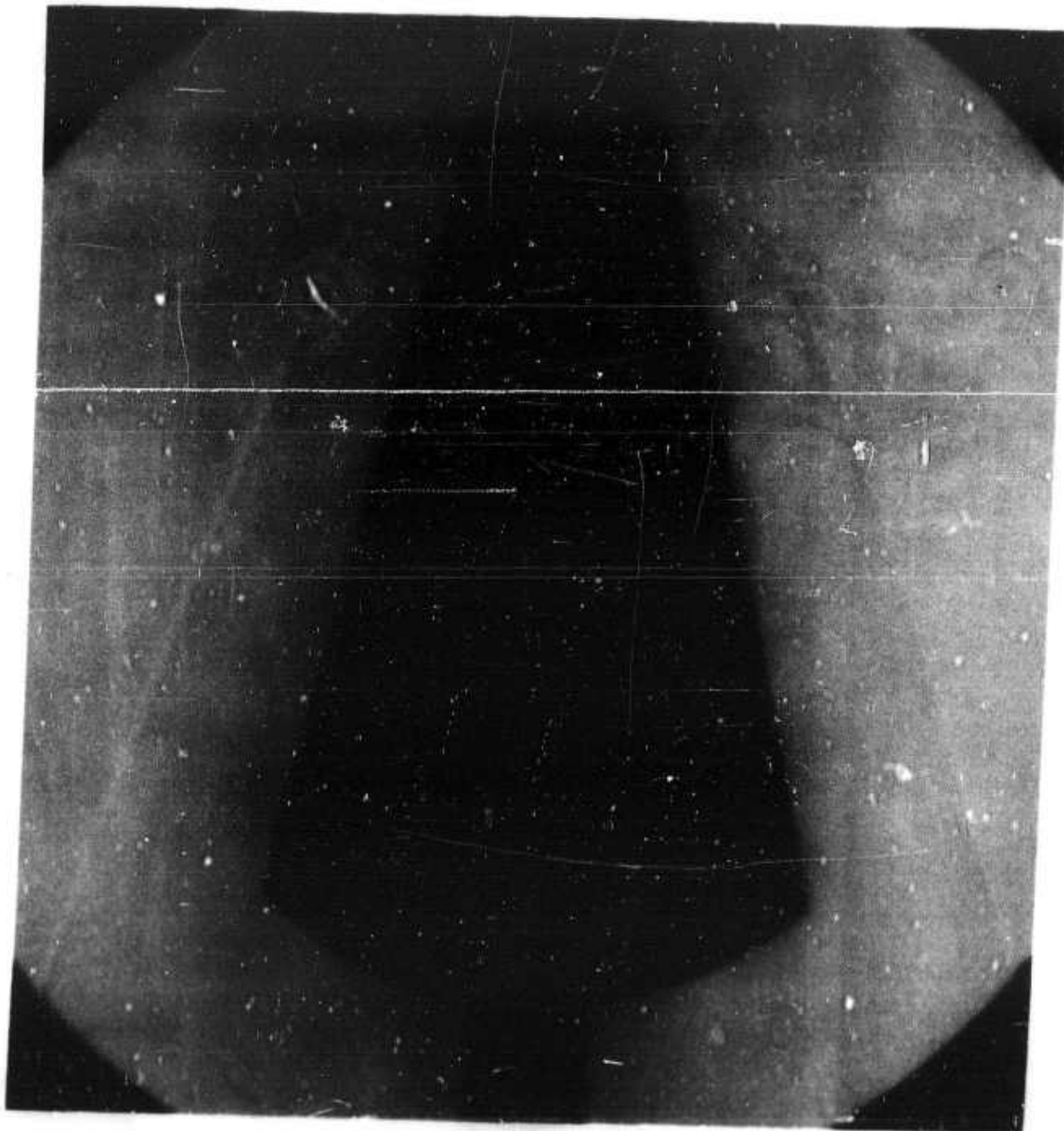
FIG.4 SCHLIEREN PHOTOGRAPH OF A
JUPITER MODEL AT M= 6.1 AND
ε=O DEGREES
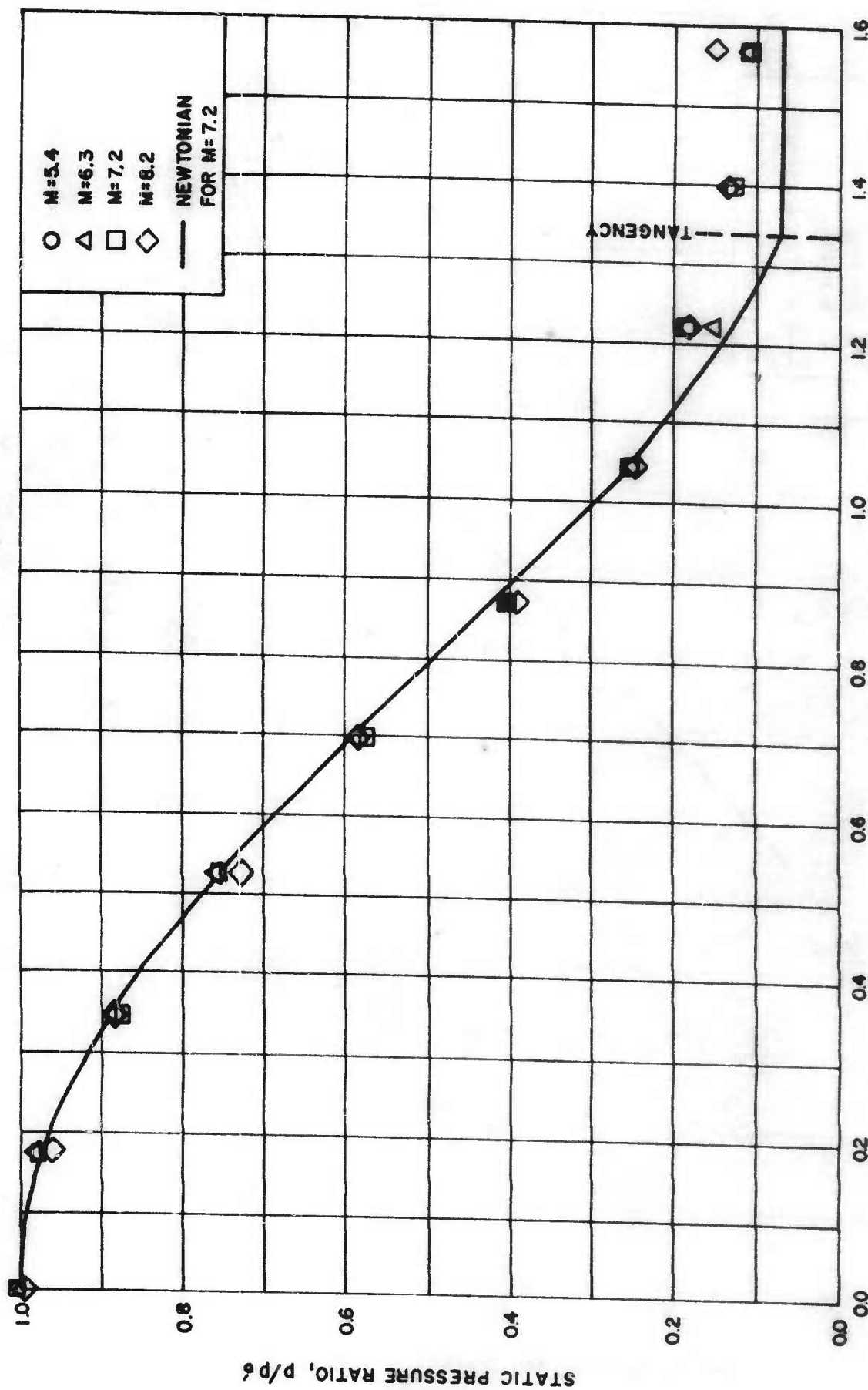
FIG. 5 PRESSURE DISTRIBUTIONS AT ZERO-YAW ON
SPHERICAL NOSE AT M=5.4, 6.3, 7.2 AND 8.2
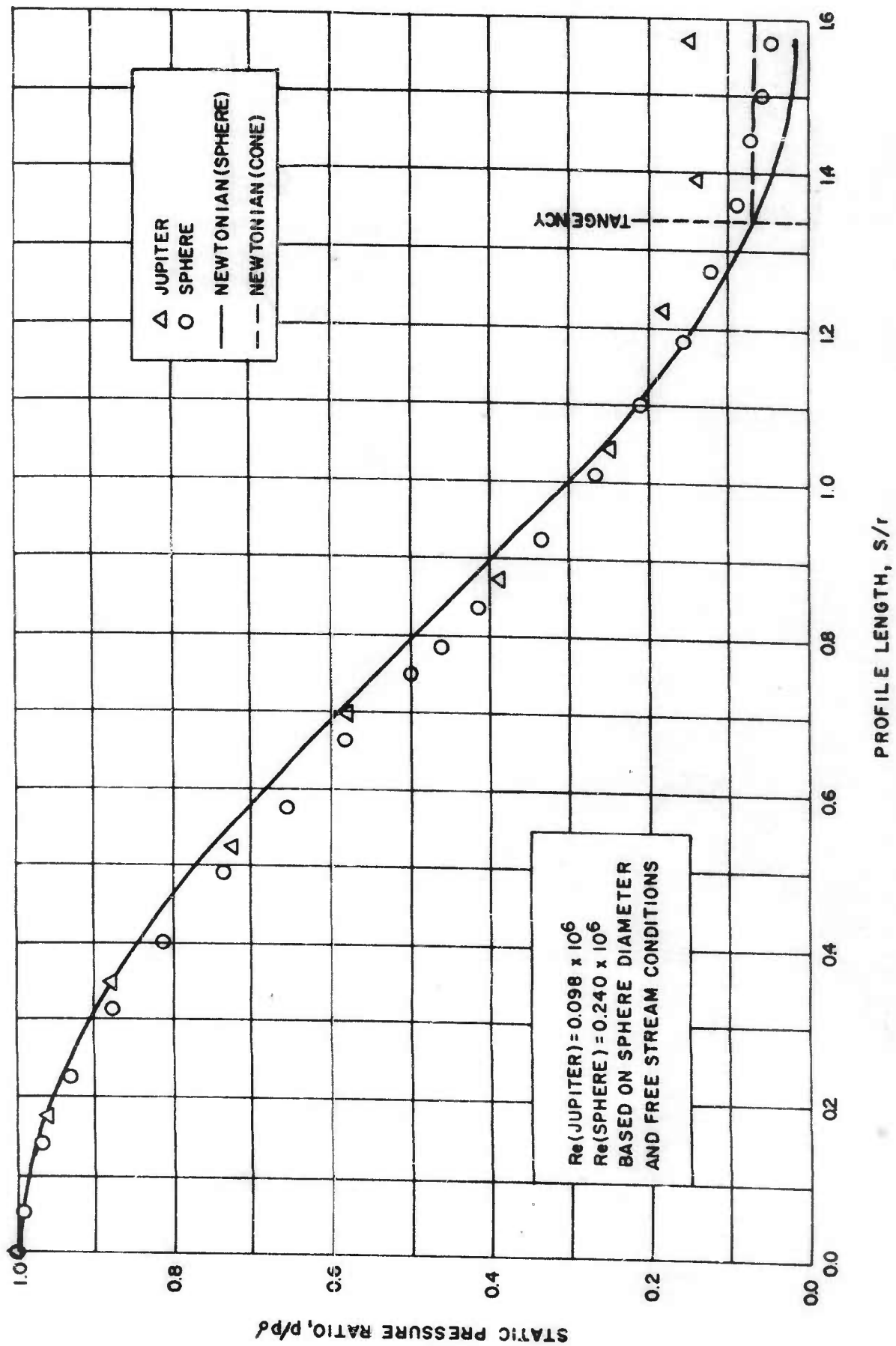
FIG. 6 COMPARISON OF PRESSURE DISTRIBUTIONS ON JUPITER SPHERICAL NOSE AND ON A SPHERE MODEL AT M=8.2
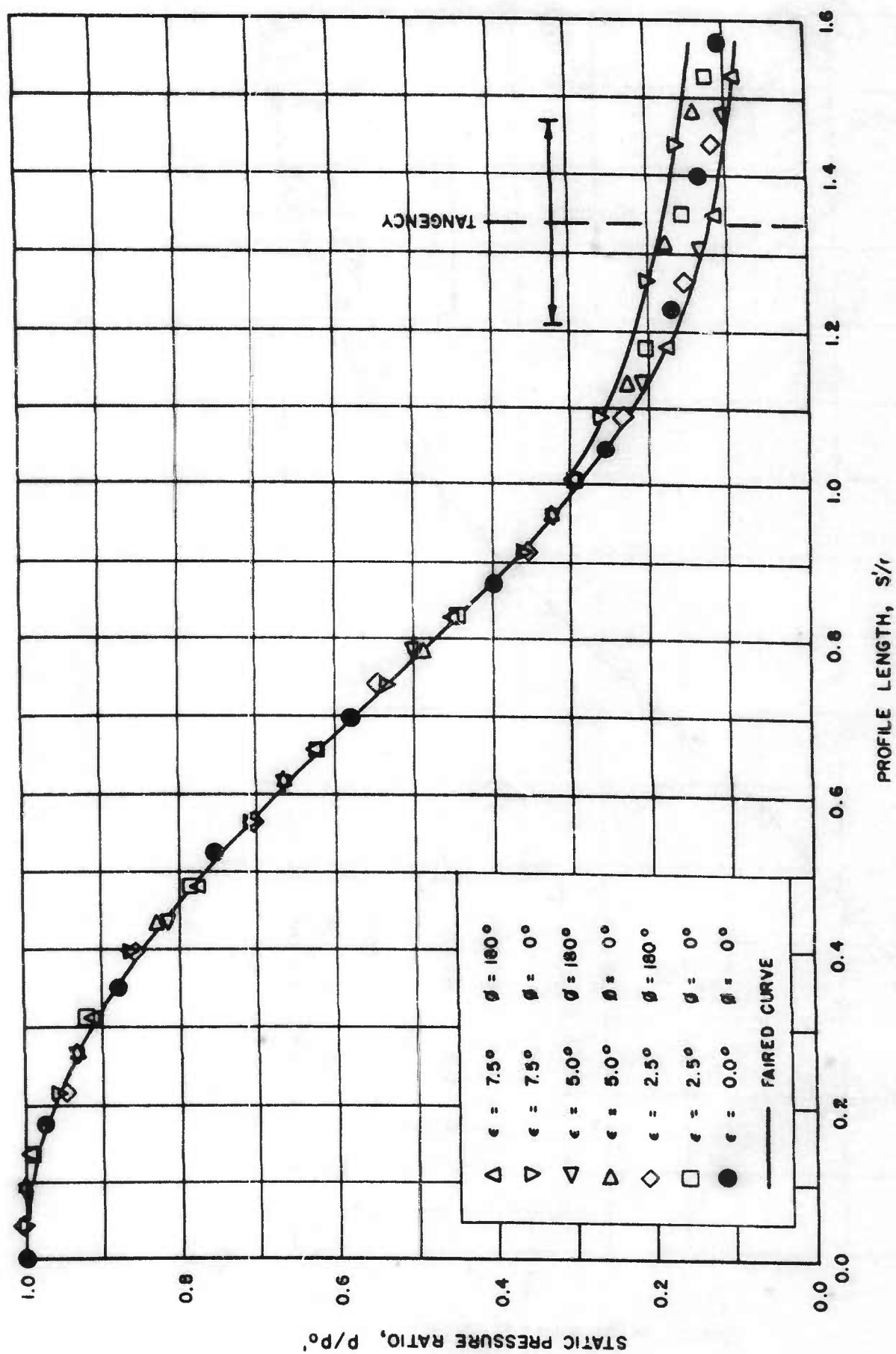
FIG. 7 PRESSURE DISTRIBUTIONS IN YAW PLANE ON SPHERICAL NOSE AT M = 5.4
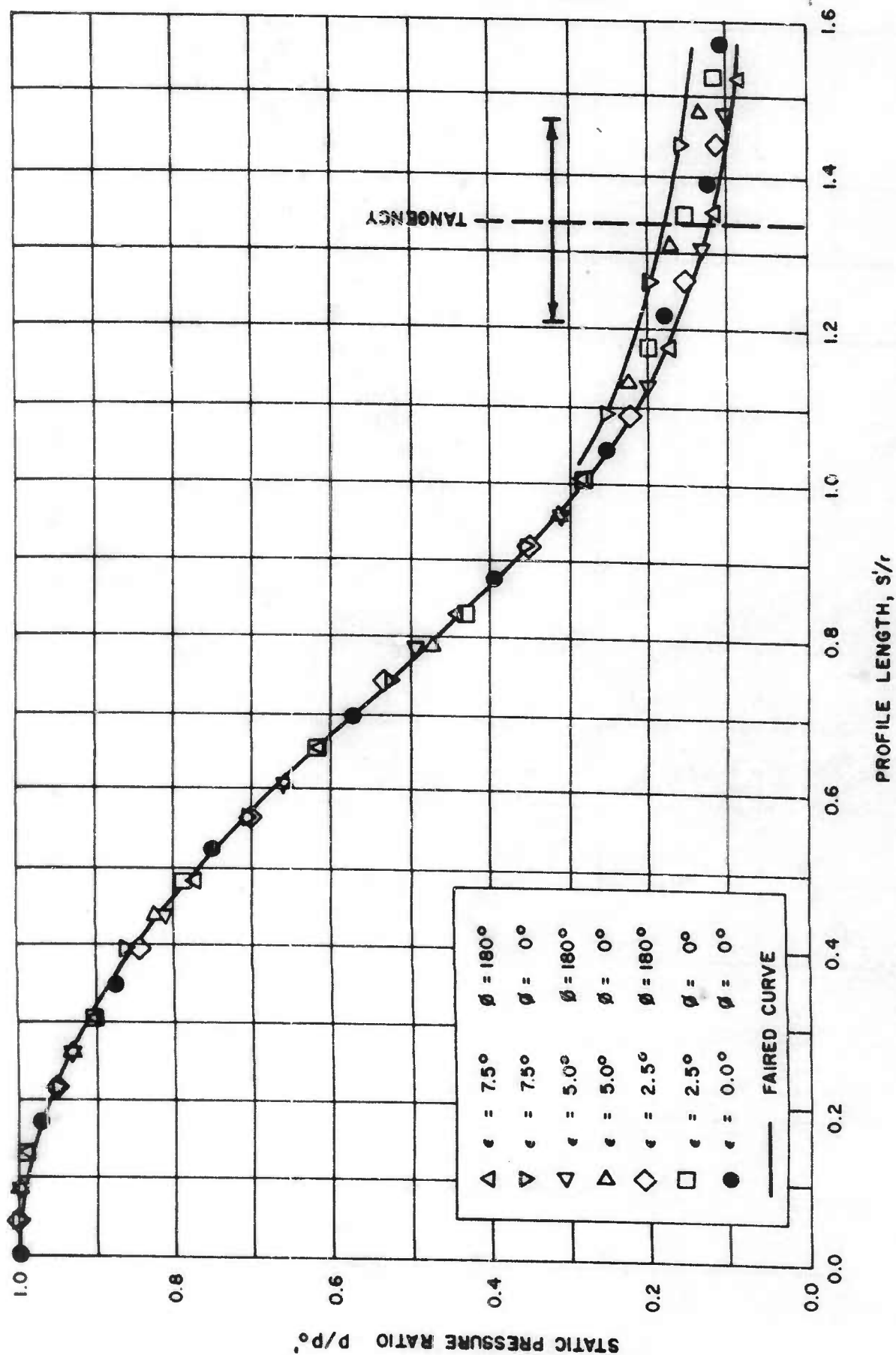
FIG. 8 PRESSURE DISTRIBUTIONS IN YAW PLANE ON
SPHERICAL NOSE AT M=6.3
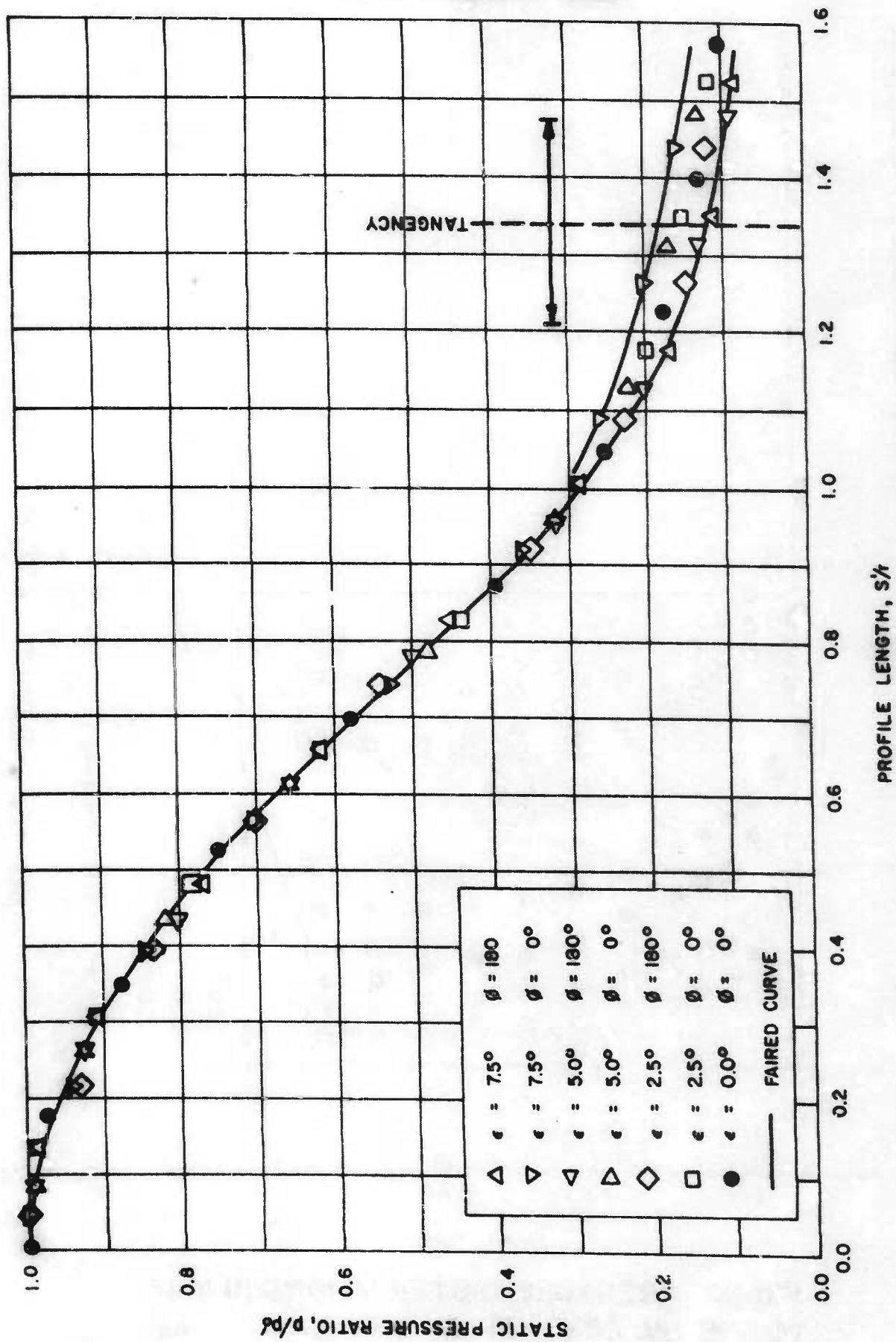
FIG. 9 PRESSURE DISTRIBUTIONS IN YAW PLANE ON
SPHERICAL NOSE AT M=7.2

FIG. 10 PRESSURE DISTRIBUTIONS IN YAW
PLANE ON CONE AT M = 5.4, 6.3 AND 7.2

FIG. 11 COMPARISON OF PRESSURE DISTRIBUTIONS ON TWO
SPHERE-CONE MODELS AT NOMINAL M=5.6
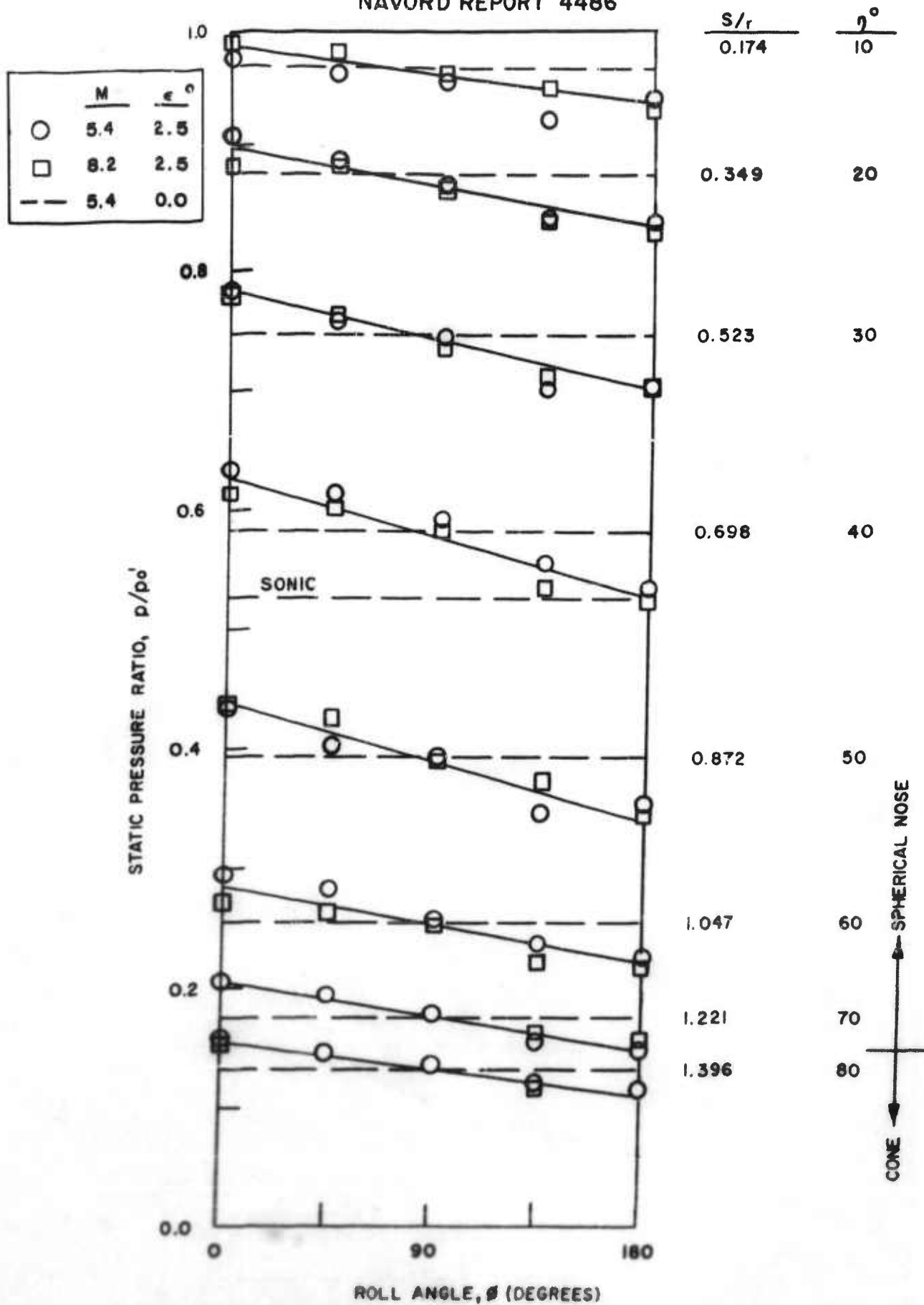
FIG. 12 TRANSVERSE PRESSURE DISTRIBUTIONS
AT M = 5.4, 8.2 AND ϵ = 2.5°

FIG. 13 TRANSVERSE PRESSURE DISTRIBUTIONS
AT M= 6.3, 7.2 AND ε = 2.5°

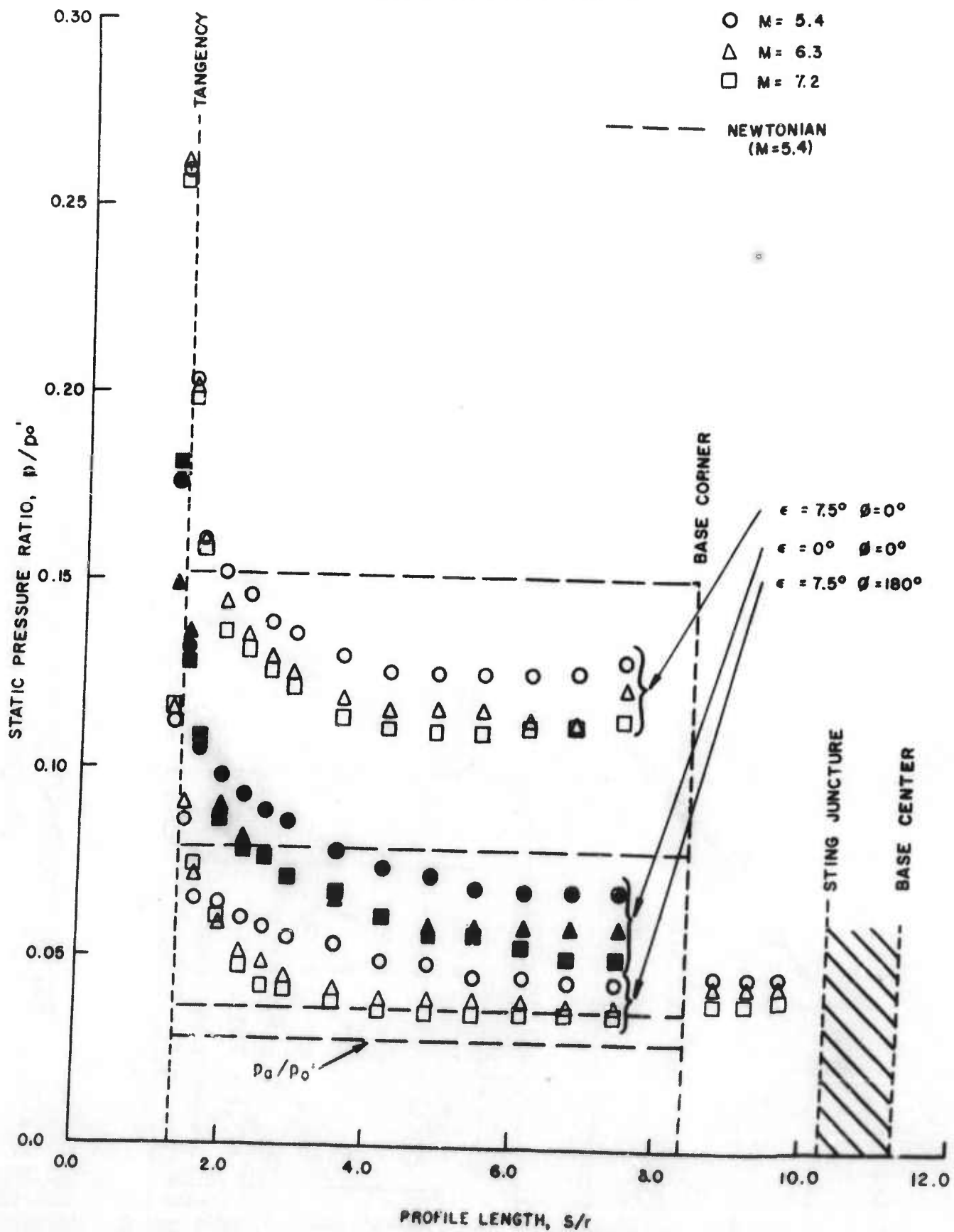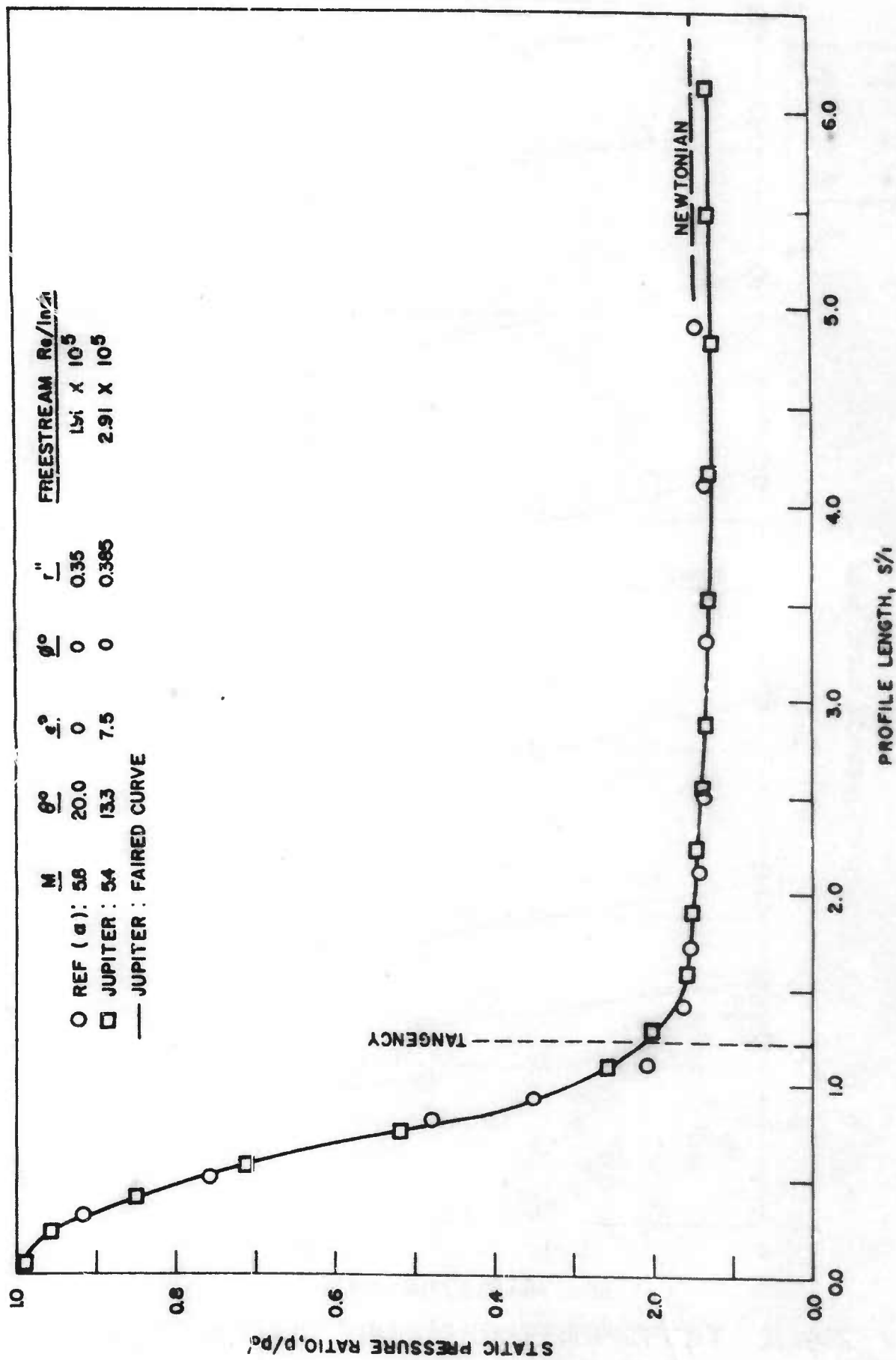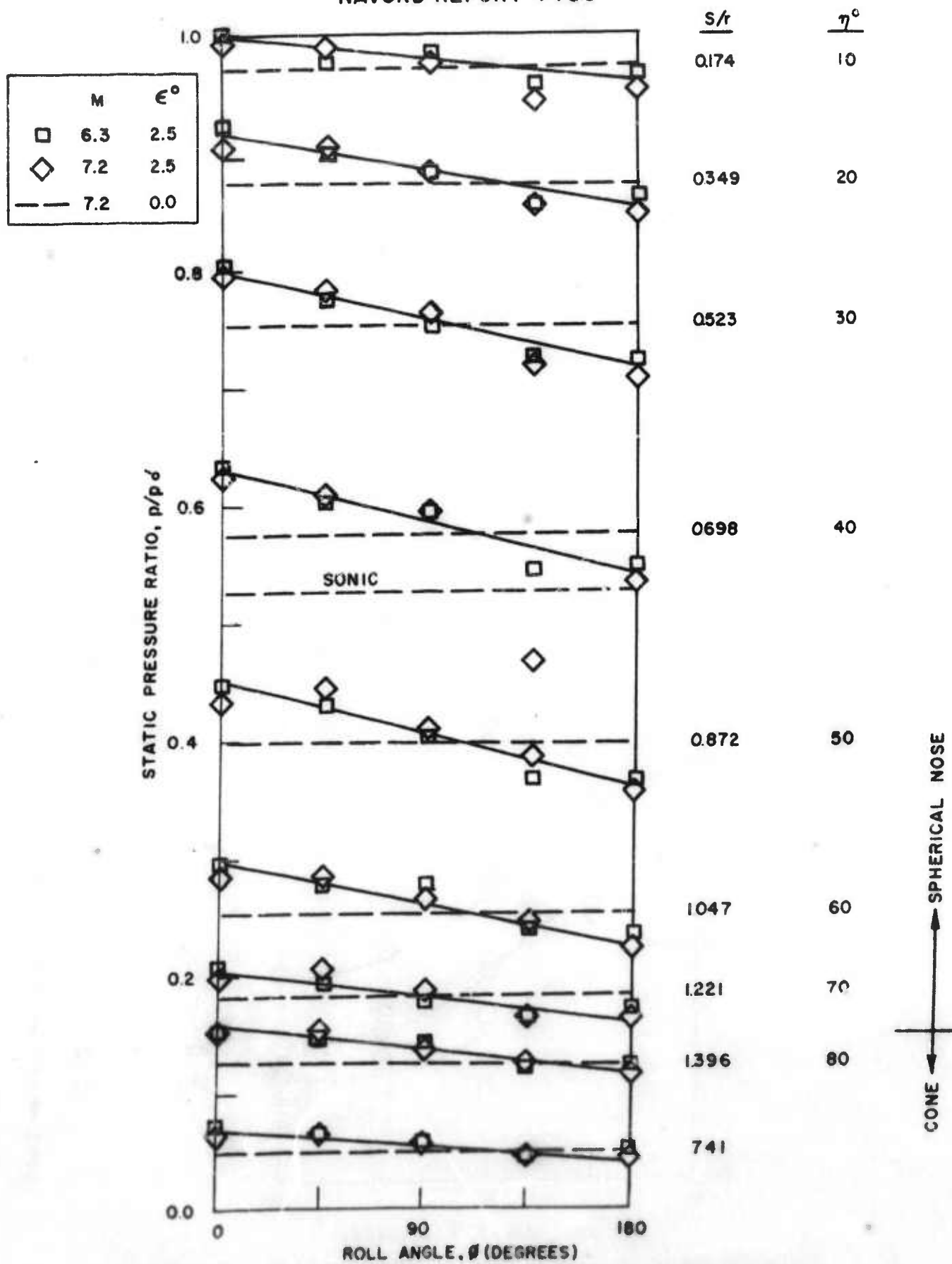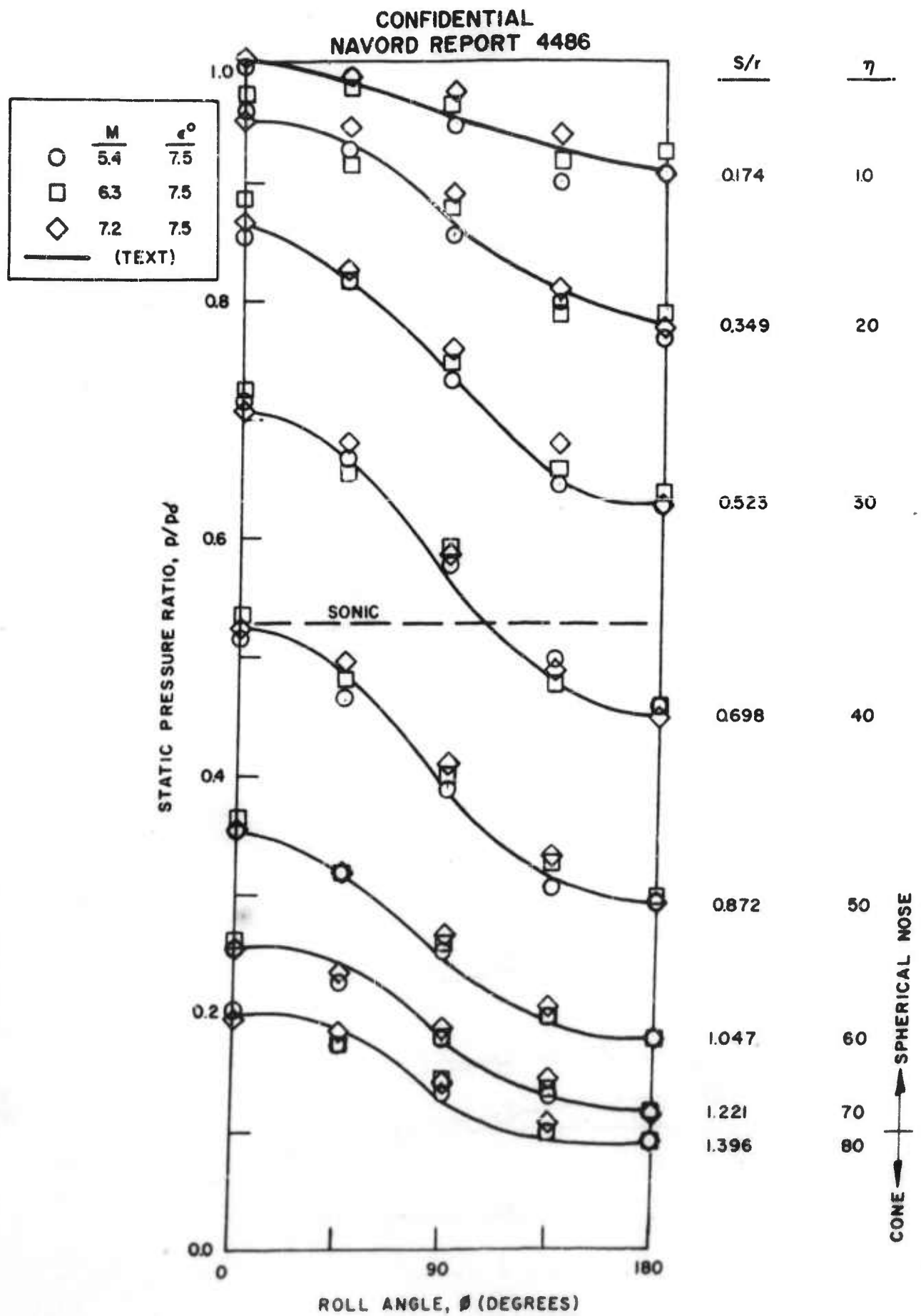FIG. 14 TRANSVERSE PRESSURE DISTRIBUTIONS
AT M=5.4, 6.3, 7.2 AND ε = 7.5°

TABLE I

P/P∞ VS S/r AT M=5.4

ROLL ANGLE, Φ	0°	0°	0°	0°	45°	45°	45°	90°	90°	90°	135°	135°	135°	180°	180°	180°
YAW ANGLE, ε	0°	2.5°	5.0°	7.5°	2.5°	5.0°	7.5°	2.5°	5.0°	7.5°	2.5°	5.0°	7.5°	2.5°	5.0°	7.5°
S/r	P/P∞	P/P∞	P/P∞	P/P∞	P/P∞	P/P∞	P/P∞	P/P∞	P/P∞	P/P∞	P/P∞	P/P∞	P/P∞	P/P∞	P/P∞	P/P∞
0	1.000	0.998	0.998	0.991	0.984	0.978	0.972	0.993	0.988	0.985	0.994	0.987	0.989	0.995	0.989	0.982
0.174	0.971	0.979	0.989	0.995	0.967	0.972	0.986	0.961	0.958	0.949	0.929	0.917	0.896	0.948	0.934	0.906
0.349	0.881	0.912	0.935	0.961	0.895	0.915	0.923	0.973	0.866	0.853	0.849	0.819	0.796	0.842	0.803	0.768
0.523	0.748	0.785	0.820	0.855	0.760	0.784	0.813	0.748	0.743	0.731	0.701	0.677	0.640	0.704	0.668	0.626
0.698	0.583	0.631	0.668	0.712	0.617	0.649	0.666	0.591	0.588	0.573	0.558	0.522	0.492	0.536	0.492	0.450
0.872	0.394	0.436	0.478	0.520	0.405	0.430	0.460	0.395	0.391	0.390	0.348	0.327	0.300	0.354	0.320	0.289
1.047	0.256	0.293	0.324	0.357	0.282	0.306	0.329	0.259	0.262	0.254	0.239	0.217	0.200	0.227	0.198	0.174
1.221	0.176	0.201	0.231	0.259	0.193	0.210	0.229	0.179	0.172	0.178	0.156	0.143	0.128	0.150	0.134	0.112
1.396	0.132	0.158	0.176	0.203	0.148	0.162	0.178	0.136	0.142	0.135	0.120	0.117	0.100	0.117	0.100	0.086
1.571	0.105	0.121	0.143	0.161	0.114	0.127	0.142	0.106	0.104	0.110	0.092	0.086	0.076	0.088	0.079	0.065
1.90	0.098	0.113	0.133	0.152	0.082	0.107	0.103	0.098	0.098	0.098	0.109	0.064	0.059	0.084	0.072	0.064
2.22	0.093	0.108	0.126	0.146	0.101	0.111	0.124	0.093	0.093	0.093	0.082	0.074	0.067	0.081	0.068	0.060
2.54	0.089	0.103	0.120	0.139	0.097	0.106	0.120	0.088	0.088	0.088	0.080	0.073	0.064	0.078	0.066	0.058
2.87	0.086	0.098	0.115	0.136	0.092	0.102	0.116	0.086	0.076	0.084	0.076	0.071	0.063	0.073	0.064	0.055
3.52	0.078	0.090	0.109	0.130	0.087	0.097	0.110	0.078	0.079	0.078	0.070	0.064	0.059	0.068	0.059	0.053
4.17	0.074	0.086	0.104	0.126	0.082	0.096	0.107	0.076	0.073	0.074	0.067	0.061	0.054	0.064	0.055	0.049
4.82	0.072	0.083	0.103	0.126	0.080	0.092	0.107	0.073	0.072	0.072	0.063	0.058	0.053	0.061	0.054	0.048
5.77	0.069	0.082	0.102	0.126	0.078	0.090	0.107	0.071	0.069	0.069	0.061	0.056	0.050	0.059	0.051	0.045
6.12	0.068	0.082	0.102	0.126	0.077	0.089	0.107	0.068	0.068	0.068	0.060	0.054	0.049	0.058	0.049	0.045
6.76	0.068	0.082	0.102	0.127	0.077	0.089	0.107	0.068	0.068	0.068	0.059	0.053	0.048	0.056	0.046	0.045
7.41	0.068	0.082	0.102	0.130	0.077	0.089	0.107	0.068	0.068	0.068	0.059	0.053	0.048	0.056	0.046	0.045
8.77	0.045	0.045	0.048	0.049	0.046	0.048	0.050	0.044	0.045	0.044	0.044	0.044	0.047	0.045	0.046	0.046
9.22	0.045	0.045	0.048	0.048	0.045	0.047	0.050	0.044	0.045	0.044	0.044	0.046	0.046	0.045	0.046	0.046
9.64	0.045	0.045	0.048	0.048	0.045	0.047	0.049	0.044	0.045	0.043	0.044	0.046	0.046	0.045	0.046	0.046

TABLE II

P_{hk} vs S/r at M=6.3

ROLL ANGLE, φ:	0°	0°	0°	0°	45°	45°	45°	90°	90°	90°	135°	135°	135°	180°	180°	180°
YAW ANGLE, ε:	0°	2.5°	5.0°	7.5°	2.5°	5.0°	7.5°	2.5°	5.0°	7.5°	2.5°	5.0°	7.5°	2.5°	5.0°	7.5°
S/r	p/p'_e	p/p'_e	p/p'_e	p/p'_e	p/p'_e	p/p'_e	p/p'_e	p/p'_e	p/p'_e	p/p'_e	p/p'_e	p/p'_e	p/p'_e	p/p'_e	p/p'_e	p/p'_e
0	1.000	1.000	0.977	0.984	1.000	1.000	0.979	1.000	1.000	1.000	1.000	1.000	0.977	1.000	1.000	1.000
0.174	0.973	0.989	1.000	1.000	0.976	0.985	0.980	0.965	0.957	0.968	0.944	0.948	0.915	0.945	0.931	0.909
0.349	0.880	0.906	0.935	0.954	0.892	0.907	0.915	0.871	0.871	0.874	0.844	0.830	0.787	0.845	0.812	0.775
0.523	0.756	0.787	0.826	0.862	0.774	0.794	0.816	0.737	0.742	0.745	0.712	0.700	0.657	0.703	0.665	0.627
0.698	0.585	0.622	0.668	0.707	0.603	0.632	0.655	0.583	0.586	0.588	0.536	0.514	0.474	0.534	0.493	0.450
0.872	0.399	0.436	0.478	0.524	0.428	0.452	0.480	0.394	0.395	0.397	0.363	0.347	0.325	0.355	0.319	0.290
1.047	0.258	0.286	0.322	0.356	0.276	0.295	0.319	0.267	0.267	0.258	0.231	0.208	0.192	0.225	0.200	0.174
1.221	0.149	0.198	0.223	0.255	0.195	0.216	0.233	0.176	0.178	0.178	0.159	0.146	0.134	0.150	0.131	0.114
1.396	0.136	0.152	0.174	0.197	0.149	0.162	0.175	0.141	0.161	0.140	0.119	0.110	0.096	0.116	0.095	0.088
1.571	0.108	0.119	0.136	0.158	0.116	0.131	0.144	0.107	0.107	0.108	0.098	0.089	0.077	0.091	0.081	0.070
1.90	0.089	0.108	0.119	0.141	0.100	0.113	0.137	0.078	0.090	0.091	0.080	0.073	0.065	0.073	0.065	0.057
2.22	0.081	0.093	0.112	0.132	0.096	0.108	0.129	0.083	0.084	0.084	0.076	0.069	0.063	0.068	0.059	0.050
2.54	0.076	0.089	0.104	0.126	0.092	0.101	0.124	0.080	0.080	0.081	0.073	0.066	0.059	0.063	0.055	0.048
2.87	0.070	0.084	0.100	0.122	0.088	0.097	0.119	0.075	0.077	0.077	0.069	0.063	0.057	0.059	0.051	0.044
3.52	0.065	0.078	0.094	0.116	0.082	0.091	0.112	0.069	0.070	0.070	0.063	0.058	0.050	0.054	0.047	0.040
4.17	0.060	0.072	0.091	0.113	0.075	0.087	0.108	0.064	0.066	0.066	0.057	0.051	0.046	0.048	0.043	0.038
4.82	0.058	0.070	0.090	0.113	0.073	0.084	0.107	0.062	0.063	0.064	0.055	0.048	0.042	0.047	0.042	0.038
5.47	0.058	0.069	0.090	0.113	0.071	0.083	0.106	0.059	0.061	0.062	0.052	0.047	0.042	0.047	0.041	0.038
6.12	0.058	0.069	0.090	0.110	0.069	0.081	0.106	0.058	0.060	0.060	0.050	0.046	0.041	0.047	0.041	0.038
6.76	0.058	0.069	0.090	0.110	0.069	0.081	0.107	0.058	0.060	0.060	0.050	0.046	0.041	0.047	0.041	0.038
7.41	0.058	0.069	0.090	0.119	0.066	0.080	0.109	0.058	0.059	0.060	0.046	0.046	0.039	0.047	0.041	0.038
8.77	0.038	0.039	0.039	0.042	0.039	0.039	0.041	0.039	0.039	0.043	0.038	0.039	0.041	0.038	0.039	0.043
9.22	0.039	0.039	0.039	0.042	0.039	0.039	0.041	0.038	0.039	0.055	0.038	0.039	0.041	0.038	0.039	0.043
9.64	0.039	0.039	0.040	—	0.039	0.039	0.041	—	—	—	0.038	0.039	0.042	0.038	0.040	0.043

TABLE III

p/p₆ VS S/r AT M = 7.2

ROLL ANGLE, θ:	0°	0°	0°	0°	45°	45°	45°	90°	90°	90°	135°	135°	135°	180°	180°	180°
YAW ANGLE, φ:	0°	2.5°	5.0°	7.5°	2.5°	5.0°	7.5°	2.5°	5.0°	7.5°	2.5°	5.0°	7.5°	2.5°	5.0°	7.5°
S/r	p/p_1	p/p_1	p/p_1	p/p_1	p/p_1	p/p_1	p/p_1	p/p_1	p/p_1	p/p_1	p/p_1	p/p_1	p/p_1	p/p_1	p/p_1	p/p_1
0	1.000	1.000	0.994	0.981	1.000	0.997	1.000	1.000	1.000	1.000	1.000	1.000	0.986	1.000	0.999	0.990
0.174	0.972	0.990	1.000	1.000	0.992	1.000	0.981	0.976	0.972	0.971	0.945	0.938	0.938	0.947	0.931	0.903
0.349	0.876	0.907	0.932	0.948	0.900	0.918	0.945	0.883	0.847	0.887	0.853	0.835	0.803	0.844	0.812	0.773
0.523	0.751	0.791	0.827	0.859	0.790	0.899	0.824	0.760	0.757	0.755	0.719	0.694	0.677	0.704	0.664	0.623
0.698	0.576	0.622	0.666	0.703	0.611	0.641	0.678	0.593	0.587	0.585	0.467	0.522	0.486	0.533	0.494	0.448
0.872	0.398	0.435	0.476	0.522	0.438	0.467	0.490	0.406	0.402	0.401	0.371	0.348	0.330	0.353	0.320	0.289
1.047	0.252	0.285	0.319	0.351	0.279	0.302	0.326	0.263	0.259	0.260	0.235	0.219	0.202	0.224	0.202	0.175
1.221	0.181	0.200	0.225	0.255	0.198	0.216	0.232	0.187	0.184	0.183	0.160	0.145	0.141	0.152	0.131	0.117
1.396	0.128	0.152	0.172	0.198	0.149	0.164	0.180	0.136	0.133	0.137	0.122	0.112	0.104	0.116	0.102	0.089
1.571	0.108	0.119	0.137	0.157	0.121	0.130	0.140	0.114	0.115	0.115	0.101	0.093	0.086	0.092	0.083	0.074
1.90	0.086	0.098	0.119	0.136	0.100	0.118	0.124	0.087	0.089	0.089	0.068	0.068	0.064	0.072	0.068	0.051
2.22	0.079	0.096	0.109	0.131	0.092	0.103	0.112	0.081	0.083	0.081	0.074	0.066	0.062	0.064	0.059	0.047
2.54	0.076	0.091	0.102	0.125	0.088	0.100	0.109	0.079	0.078	0.076	0.068	0.062	0.057	0.059	0.056	0.042
2.87	0.071	0.087	0.097	0.121	0.083	0.093	0.105	0.075	0.073	0.072	0.064	0.059	0.055	0.056	0.053	0.041
3.52	0.057	0.087	0.091	0.114	0.078	0.088	0.101	0.069	0.069	0.065	0.061	0.053	0.049	0.048	0.049	0.039
4.17	0.061	0.071	0.087	0.110	0.072	0.082	0.096	0.066	0.065	0.060	0.058	0.049	0.047	0.045	0.044	0.036
4.82	0.056	0.069	0.082	0.110	0.068	0.079	0.093	0.063	0.062	0.057	0.055	0.047	0.046	0.043	0.043	0.035
5.47	0.056	0.066	0.082	0.110	0.066	0.077	0.093	0.060	0.057	0.057	0.051	0.045	0.044	0.043	0.043	0.035
6.12	0.053	0.065	0.082	0.110	0.065	0.076	0.093	0.060	0.056	0.056	0.048	0.045	0.038	0.043	0.041	0.035
6.76	0.050	0.065	0.082	0.111	0.065	0.077	0.093	0.060	0.056	0.056	0.048	0.044	0.038	0.045	0.039	0.035
7.41	0.050	0.064	0.082	0.114	0.065	0.077	0.096	0.058	0.056	0.056	0.047	0.043	0.037	0.045	0.037	0.035
8.77	0.032	0.033	0.036	0.038	0.033	0.036	0.038	0.039	0.033	0.036	0.032	0.033	0.040	0.033	0.036	0.039
9.22	0.032	0.033	0.036	0.038	0.033	0.036	0.038	0.033	0.036	0.039	0.032	0.036	0.040	0.033	0.036	0.039
9.64	0.032	0.033	0.036	0.038	0.034	0.036	0.038	0.034	0.036	0.039	0.033	0.036	0.040	0.033	0.036	0.040

TABLE IV

p/p'₀ VS s/r AT M=8.2

ROLL ANGLE, φ:	0°	0°	45°	90°	135°	180°
YAW ANGLE, ε:	0°	2.5°	2.5°	2.5°	2.5°	2.5°
s/r	p/p'₀	p/p'₀	p/p'₀	p/p'₀	p/p'₀	p/p'₀
0	1.000	0.989	0.997	1.000	1.000	1.000
0.174	0.967	0.991	0.982	0.966	0.955	0.935
0.349	0.887	0.887	0.888	0.873	0.843	0.830
0.523	0.731	0.785	0.766	0.736	0.711	0.701
0.698	0.584	0.611	0.600	0.581	0.536	0.521
0.872	0.392	0.437	0.425	0.390	0.371	0.342
1.047	0.249	0.270	0.261	0.254	0.221	0.217
1.221	0.181	0.206	0.196	0.179	0.164	0.158
1.396	0.139	0.150	0.143	0.137	0.118	0.114
1.571	0.151	0.199	0.186	0.142	0.144	0.087
1.90	0.095	0.195	0.104	0.094	0.085	0.071
2.22	0.086	0.097	0.095	0.085	0.077	0.070
2.54	0.080	0.090	0.088	0.079	0.071	0.065
2.87	0.073	0.086	0.082	0.074	0.067	0.064
3.52	0.070	0.078	0.076	0.070	0.060	0.056
4.17	0.073	0.072	0.070	0.072	0.055	0.049
4.82	0.085	0.069	0.068	0.077	0.052	0.048
5.47	0.091	0.076	0.065	0.082	0.049	0.038
6.12	0.095	0.093	0.064	0.086	0.047	0.043
6.76	0.093	0.144	0.064	0.084	0.046	0.049
7.41	0.104	0.270	0.063	0.090	0.045	0.050
8.77	0.027	——	0.030	0.023	0.030	0.031
9.22	0.027	——	0.030	——	0.030	0.027
9.64	0.025	——	0.030	——	0.029	0.028